Effects of initial system-environment correlations on open-quantum-system dynamics and state preparation

Chien-Chang Chen and Hsi-Sheng Goan*
Department of Physics and Center for Theoretical Sciences, National Taiwan University, Taipei 10617, Taiwan
and Center for Quantum Science and Engineering, National Taiwan University, Taipei 10617, Taiwan
(Received 15 September 2015; published 9 March 2016)

We investigate the preparation of a target initial state for a two-level (qubit) system from a system-environment equilibrium or correlated state by an external field. The system-environment equilibrium or correlated state results from the inevitable interaction of the system with its environment. An efficient method in an extended auxiliary Liouville space is introduced to describe the dynamics of the non-Markovian open quantum system in the presence of a strong field and an initial system-environment correlation. By using the time evolutions of the population difference, the state trajectory in the Bloch sphere representation, and the trace distance between two reduced system states of the open quantum system, the effect of initial system-environment correlations on the preparation of a system state is studied. We introduce an upper bound and a lower bound for the trace distance within our perturbation formalism to describe the diverse behaviors of the dynamics of the trace distance between various correlated states after the system state preparation. These bounds, that are much more computable than similar bounds in the literature, give a sufficient condition and a necessary condition for the increase of the trace distance and are related to the witnesses of non-Markovianity and initial system-bath correlation.

DOI: 10.1103/PhysRevA.93.032113

I. INTRODUCTION

Besides precise coherent control, the ability to prepare initial states of quantum systems accurately is also one of the essential requirements for quantum information processing. Most of the state preparations implemented in quantum experiments assume having ideal (closed) quantum coherent systems. However, almost every quantum system interacts inevitably with its surrounding environment (bath), resulting in an equilibrium or correlated system-environment state before any operation or measurement of the system is performed [1–6]. Thus how to prepare a desired initial system state from an equilibrium or correlated system-environment state becomes an important and practical issue [7–10].

In addition to its effect on the system dynamics, system-environment correlation also plays a vital role in quantum dynamical maps and open-system state distinguishability [6,11–35]. The reduced dynamics of an open quantum system with a tensor product (factorized) initial system-environment state is a completely positive map. Completely positive maps are appealing because they form a time-dependent semigroup and have a simple mathematical structure: the composition of two completely positive maps is also a completely positive map [2,3,36,37]. This makes the initial factorization of the joint system-environment state an attractive and commonly adopted initial condition when studying the dynamics of an open quantum system. However, when the system-environment interaction is not very weak, the initial system-environment correlation may have an appreciable effect on the open-system dynamics.

References [9,10] have investigated the role of initial system-environment correlations on the reduced system dynamics with a system state initially prepared by a projective (selective) measurement on the system alone. The system-environment state before the projective measurement is a total thermal equilibrium state $\rho_T^{\rm eq} = e^{-\beta H_T}/{\rm tr}_T e^{-\beta H_T}$, where H_T is the total Hamiltonian, including the system-environment interaction Hamiltonian. The projective measurement is assumed to be instantaneous such that the (unnormalized) environment state after the measurement collapses to $\langle\psi|\rho_T^{\rm eq}|\psi\rangle$, conditioned on the projected system state $|\psi\rangle$. The measurement has the effect of removing the system-environment correlation, and this measurement-induced factorized initial system-environment state has been considered in the literature [9,10,27,38–40]. However, in practice, if the post-measurement system state evolution is of interest or concern, the measurement made upon the system is usually nondestructive and indirect, and thus takes some finite time to project the system state to the desired state $|\psi\rangle$. In other words, unless the measurement is very strong, the system and environment will evolve away from the total equilibrium state when the measurement is completed. In this case, the post-measurement density matrix of the environment is no longer $\langle\psi|\rho_T^{\rm eq}|\psi\rangle$. As a result, the system state preparation by projective measurement with the above instantaneously measurement-induced factorized system-environment state is an idealization. We note again that the subsequent system evolution is dependent on the initial system-environment correlations, but the initial system-environment state used for the investigations [9,10,27,38–40] is, however, a factorized state.

In this paper, we investigate an alternative method for state preparation by applying an external field. We use the time evolution of the trace distance [4–6,15,28,31,32] between two reduced system states of an open quantum system as a measure of the effect of initial correlations. The time evolution of the trace distance between the quantum states evolving from two kinds of initial states—a correlated total equilibrium state (or Gibbs state) and its uncorrelated marginal state—for an open

*goan@phys.ntu.edu.tw

qubit system with a week external driving field was calculated by the rotating-wave approximation (RWA) in Ref. [28]. The open-quantum-system model considered in Ref. [28] before the application of an external driving field is a pure-dephasing spin-boson model in which the system operator coupling to the environment commutes with the system Hamiltonian. However, for the purpose of accurate state preparations in open quantum systems, fast control and thus stronger fields beyond the RWA may be necessary.

The main purposes of this paper is to investigate under what conditions the initial factorization approximation of the system-environment state is valid and how different the system dynamics is when the initial system-environment correlation is taken into account, especially for state preparation via applying an external field. We will also investigate the conditions for the breakdown of the RWA and the onset of non-RWA corrections for state preparation. We go beyond the limitations or approximations imposed in Ref. [28] by considering a noncommuting spin-boson model in an external driving field without making the RWA. The method presented here to derive the time-nonlocal master equation to second order in the system-bath interaction and to take the initial correlation into account is based on the Nakajima-Zwanzig projection operator technique [2,41]. To deal with the application of a strong external field, an efficient formulation of introducing auxiliary density matrices in an extended Liouville space to transform the time-nonlocal time-ordered integro-differential master equation into a set of time-local coupled differential equations is employed. We find that when the driving field strength is above a certain value the RWA becomes invalid, and when the system-environment interaction is above a certain value the initial system-environment correlation become important to the open-system dynamics. The detailed values in relation to the fidelity or error of the state preparation will be discussed and presented.

We will also investigate the effects of the system-environment correlation established after the state preparation on the subsequent field-free system evolution. The dynamics of the trace distance has been used to study noncontractivity and non-Markovianity [15,26,32,42,43], both of which could be induced by initial correlations. We find that the dynamics of the trace distances between these correlated states and between these correlated states and their corresponding factorized states in the subsequent field-free evolutions exhibit diverse behaviors. So another purpose of the paper is to introduce an upper bound and a lower bound for the trace distance within our perturbation formalism to describe the various behaviors of the dynamics of the trace distance. These bounds that we introduce are much more computable than similar bounds in the literature [31–34]. These bounds in turn give a sufficient condition and a necessary condition for the increase of the trace distance and are related to the witnesses of non-Markovianity and initial system-bath correlations.

The paper is organized as follows. In Sec. II we describe briefly the Hamiltonian of the spin-boson model we study and the decomposition of the initially correlated state using the projection operator technique. An efficient method is introduced in Sec. III to transform the time-nonlocal master equation, with an external driving field and initial system-environment correlations accounted for, to a set of coupled linear time-local equations of motion in an extended auxiliary Liouville space. Numerical results and discussions are presented in Sec. IV. In Sec. IV A, we describe how to achieve and express the total thermal equilibrium state as an initially correlated state in the extended Liouville space formulation. The results of comparing the initially correlated state with the factorized states in terms of time evolutions of the trace distance between them for state preparation with an external driving field are presented in Sec. IV B. After the state preparation by applying an external field, the resultant correlated system-environment states are considered as the initial states for subsequent field-free evolutions. The diverse behaviors of the dynamics of the trace distance between these correlated initial states in the subsequent field-free evolutions are shown in Sec. IV C. The upper and lower bounds of the trace distance similar to those in Refs. [31–34] are introduced in Sec. V to analyze these behaviors. Finally, a conclusion is presented in Sec. VI.

II. INITIAL SYSTEM-ENVIRONMENT CORRELATION

The total Hamiltonian of the dissipative spin-boson model considered here to study the initial correlations is

$$H_T(t) = H_s(t) + H_b + H_{sb}, \tag{1}$$

with the two-level (qubit) system Hamiltonian $H_s(t)$, the bath (environment) Hamiltonian H_b, and the system-bath interaction Hamiltonian H_{sb} given respectively by ($\hbar = 1$)

$$H_s(t) = \Omega\sigma_z + H_d(t), \tag{2}$$

$$H_b = \sum_i \omega_i b_i^\dagger b_i, \tag{3}$$

$$H_{sb} = \sigma_x B. \tag{4}$$

Here σ_i with $i = x,y,z$ are the Pauli matrices, ω_i and $b_i^\dagger$ (b_i) are, respectively, the frequency and the creation (annihilation) operator of the bath mode i. The bath operator B in the the system-bath interaction is $B = \sum_i g_i(b_i^\dagger + b_i)$ with the coupling constant g_i for the respective bath mode i. The Hamiltonian $H_d(t)$ accounts for the Hamiltonian of the applied time-dependent external driving field,

$$H_d(t) = \Omega_R \cos(\omega_L t)\sigma_x, \tag{5}$$

where Ω_R is the field strength, also called the Rabi frequency, and ω_L is the field frequency.

Due to unavoidable interaction between a quantum system and its surrounding bath, the initial state considered at time $t = 0$ before performing any operation is the correlated total thermal equilibrium state,

$$\rho_T^{\rm eq} = e^{-\beta H_T}/{\rm tr}_T e^{-\beta H_T}, \tag{6}$$

where H_T is the total Hamiltonian without the driving Hamiltonian $H_d(t)$.

The projection operator technique of Nakajima-Zwanzig [2] will be used to derive the equation of motion of the reduced system dynamics with the initial system-environment correlation accounted for. In this formalism, the projection superoperator P acting on the total system-environment state separates the bath from the system via $P\rho_T(t) = {\rm tr}_b[\rho_T(t)] \otimes$

$\rho_b = \rho_s(t) \otimes \rho_b$, where ρ_b is some fixed state of the environment which we take as the bath thermal equilibrium state, i.e., $\rho_b = e^{-\beta H_b}/\mathrm{tr}_b e^{-\beta H_b}$, and we have used the fact that $\rho_s(t) = \mathrm{tr}_b[\rho_T(t)]$ is the density matrix operator of the reduced system obtained by tracing the total density matrix operator over the bath degrees of freedom. The projection superoperator P and a complementary superoperator Q satisfy the following properties: $P + Q = \mathcal{I}$, $P^2 = P$, $Q^2 = Q$, and $PQ = QP = 0$, where $\mathcal{I}$ is an identity operator in the joint total system-environment state space. Any total system-environment state $\rho_T(t)$ can be expressed as

$$\mathcal{I}\rho_T(t) = P\rho_T(t) + Q\rho_T(t) = \rho_s(t) \otimes \rho_b + Q\rho_T(t). \quad (7)$$

The bath (environment) thermal equilibrium state ρ_b serves as the bath reference state and is the bath state of the factorized system-bath states used throughout this paper. Thus the total initial state can also be expressed as

$$\rho_T(0) = \rho_s(0) \otimes \rho_b + Q\rho_T(0) \quad (8)$$

that contains a factorized part $\rho_s(0) \otimes \rho_b$ and a nonfactorized part $Q\rho_T(0)$.

III. TIME-NONLOCAL MASTER EQUATION

Next we present the time-nonlocal master equation that incorporates the initial system-environment correlation. The equation of motion for the total density matrix is given by

$$\dot{\rho}_T(t) = -i[H_T(t), \rho_T(t)]. \quad (9)$$

Defining the density matrix of the reduced system as

$$\rho_s(t) = \mathrm{tr}_b[\rho_T(t)] = \mathrm{tr}_b[\mathcal{G}_T(t,0)\rho_T(0)], \quad (10)$$

one can formally write

$$\dot{\rho}_s(t) = (-i)\mathrm{tr}_b[H_T(t), \rho_T(t)] \quad (11)$$

$$\equiv \mathrm{tr}_b[\mathscr{L}_T(t)\rho_T(t)]. \quad (12)$$

Here the propagator superoperator has a general form of

$$\mathcal{G}_j(t,t') \equiv T_+ \exp\left[\int_{t'}^{t} \mathscr{L}_j(t'')dt''\right] \quad (13)$$

with T_+ denoting the time-ordering operator necessary to allow an explicit time-dependent Hamiltonian [2,41], and the Liouville superoperator

$$\mathscr{L}_j(t)A \equiv -i[H_j(t), A] \quad (14)$$

defined as commutator between any operator A and $H_j(t)$ with $j = T$ for the present case. Later we will introduce $\mathscr{L}_s$ and corresponding $\mathcal{G}_s(t,t')$ for the system alone defined as in Eqs. (14) and (13) but with the replacement of Hamiltonian $H_j(t) \to H_s(t)$. It is then straightforward to verify that

$$\frac{\partial}{\partial t}\mathcal{G}_j(t,t') = \mathscr{L}_j(t)\mathcal{G}_j(t,t'). \quad (15)$$

After applying the projector operators P, Q to Eq. (9) and taking terms up to second order in system-bath interaction strength, one obtains the time-convolution (time-nonlocal) master equation in the interaction picture [2]:

$$\dot{\tilde{\rho}}_s(t) = -i\mathrm{tr}_b[\tilde{H}_{sb}(t), Q\rho_T(0)] - \int_0^t \mathrm{tr}_b[\tilde{H}_{sb}(t), [\tilde{H}_{sb}(t'), \tilde{\rho}_s(t') \otimes \rho_b]]dt', \quad (16)$$

where $\tilde{\rho}_s(t) = \mathcal{G}_s(0,t)\rho_s(t)$, $\tilde{H}_{sb}(t) = \tilde{\sigma}_x(0,t)B(t)$, $\tilde{\sigma}_x(0,t) = \mathcal{G}_s(0,t)\sigma_x$, and $B(t) = \sum_i g_i(b_i^\dagger e^{i\omega_i t} + b_i e^{-i\omega_i t})$. So the nonfactorized part $Q\rho_T(0)$ in Eq. (8) now plays a role of an inhomogeneous term in the master equation. Since there is already an interaction Hamiltonian $\tilde{H}_{sb}(t)$ in the first term on the right-hand side of Eq. (16), we only need to keep $Q\rho_T(0)$ to first order in $\tilde{H}_{sb}$. The initial correlated thermal equilibrium state, Eq. (8), to first order in the system-bath interaction Hamiltonian before turning on the external field is [41]

$$\rho_T(0) = \rho_T^{\mathrm{eq}} \quad (17)$$

$$\simeq (\rho_s^{\mathrm{eq}} \otimes \rho_b)\left(1 - \int_0^\beta \tilde{H}_{sb}(-i\beta')d\beta'\right), \quad (18)$$

where $\rho_s^{\mathrm{eq}} = e^{-\beta H_s}/\mathrm{tr}_s e^{-\beta H_s}$ and $\tilde{H}_{sb}(-i\beta') = e^{\beta'(H_s+H_b)}H_{sb}e^{-\beta'(H_s+H_b)}$. The first term of Eq. (18) is the commonly used initial product system-environment state and the second term is the first-order nonfactorized part $Q\rho_T(0)$ of the total thermal equilibrium state. Tracing over the bath degrees of freedom in Eq. (16), and going back to Schrödinger picture, we arrive at [41,44]

$$\dot{\rho}_s(t) = \mathscr{L}_s(t)\rho_s(t) + \mathscr{L}_x[\mathcal{K}(t) + \mathcal{K}^\dagger(t)], \quad (19)$$

$$\mathcal{K}(t) = -i\int_{-\infty}^{t} C(t-t')\mathcal{G}_s(t,t')\sigma_x\rho_s(t')dt', \quad (20)$$

where $\rho_s(t' \leqslant 0) = \rho_s^{\mathrm{eq}}$, $\mathscr{L}_x\mathcal{K}(t) = -i[\sigma_x, \mathcal{K}(t)]$, and the bath correlation function is given by [1,2,41]

$$C(t-t') \equiv \mathrm{tr}_b[B(t)B(t')\rho_b] = \int_0^\infty d\omega\, J(\omega)\cos[\omega(t-t')]\coth\left(\frac{\beta\omega}{2}\right) - i\int_0^\infty d\omega\, J(\omega)\sin[\omega(t-t')], \quad (21)$$

with spectral density $J(\omega) = \sum_i g_i^2\delta(\omega - \omega_i)$. The integral from $t = -\infty$ to $t = 0$, i.e., $\mathcal{K}(0)$ in Eq. (20), comes from the first term on the right-hand side of Eq. (16) due to the nonfactorized contribution $Q\rho_T(0)$ of the initial system-bath state at $t = 0$ and indicates that the inhomogeneous term is the past memory of the homogeneous term in the memory kernel of the master equation.

To deal with the time-nonlocal time-ordered integro-differential master equation with a time-dependent driving Hamiltonian without making the RWA, we express the bath correlation function as a sum of exponentials [41,44–47]

$$C(t-t') = \sum_k \alpha_k e^{\gamma_k(t-t')} \quad (22)$$

with complex numbers α_k and γ_k obtained from numerical methods. By inserting Eq. (22) into

Eq. (20), one then obtains $\mathcal{K}(t)=\sum_k \mathcal{K}_k(t)$, where $\mathcal{K}_k(t)=-i\int_{-\infty}^{t}\alpha_k e^{\gamma_k(t-t')}\mathcal{G}_s(t,t')\sigma_x\rho_s(t')dt'$. By taking the time derivative of $\mathcal{K}_k(t)$ with the help of the property $\frac{\partial}{\partial t}\mathcal{G}_s(t,t')=\mathscr{L}_s(t)\mathcal{G}_s(t,t')$, Eqs. (19) and (20) now become a set of coupled linear time-local equations:

$$\dot{\rho}_s(t)=\mathscr{L}_s(t)\rho_s(t)+\mathscr{L}_x\sum_k[\mathcal{K}_k(t)+\mathcal{K}_k^{\dagger}(t)], \tag{23}$$

$$\dot{\mathcal{K}}_k(t)=[\mathscr{L}_s(t)+\gamma_k]\mathcal{K}_k(t)-i\alpha_k\sigma_x\rho_s(t). \tag{24}$$

Equations similar to $\mathcal{K}_k(t)$ hold for the Hermitian conjugate $\mathcal{K}_k{}^{\dagger}(t)$. Compared to solving the reduced density matrix of the system $\rho_s(t)$ directly through Eqs. (19) and (20), the resultant coupled differential equations for $\{\rho_s(t),\mathcal{K}_k,\mathcal{K}_k{}^{\dagger};k=1,2,3,\dots\}$ are easy to solve as they are time-local and free from the time-ordering and memory kernel integration problems. The factorized part of the initial condition at $t=0$ is $\rho_s(0)$, and the nonfactorized part of the initial condition is $\mathcal{K}_k(0)$ and $\mathcal{K}_k^{\dagger}(0)$. If $Q\rho_T(0)=0$, i.e., the initial system-bath state is in fact a factorized state, $\mathcal{K}_k(0)=\mathcal{K}_k^{\dagger}(0)=0$.

IV. NUMERICAL RESULTS

We use the trace distance, a measure of distance between two quantum states, to quantify and discuss our results. Formally, the trace distance is defined as distinguishability between two states $\rho^{\alpha},\rho^{\beta}$ by the expression [26,42]

$$D(\rho^{\alpha},\rho^{\beta})=\frac{\|\rho^{\alpha}-\rho^{\beta}\|}{2}=\frac{1}{2}\mathrm{tr}\sqrt{(\rho^{\alpha}-\rho^{\beta})^2}. \tag{25}$$

It can be shown that the trace distance between two reduced system states $\rho_s^{\alpha}(t)$ and $\rho_s^{\beta}(t)$ of a qubit system at time t in two-dimensional Hilbert space has the following form [15]:

$$\begin{aligned}D\big(\rho_s^{\alpha}(t),\rho_s^{\beta}(t)\big)&=\frac{1}{2}\big\|\Delta\rho_s^{\alpha,\beta}(t)\big\|=\frac{1}{2}\mathrm{tr}\sqrt{\big[\Delta\rho_s^{\alpha,\beta}(t)\big]^2}\\&=\sqrt{\big(\Delta\rho_{11}^{\alpha,\beta}(t)\big)^2+\big|\Delta\rho_{12}^{\alpha,\beta}(t)\big|^2},\end{aligned} \tag{26}$$

where $\Delta\rho_j^{\alpha,\beta}(t)=\rho_j^{\alpha}(t)-\rho_j^{\beta}(t)$ with subscript $j=s$ for the reduced system density matrix and $j=11,12$ for the matrix elements of

$$\rho_s(t)=\begin{pmatrix}\rho_{11}(t) & \rho_{12}(t)\\ \rho_{12}^{*}(t) & 1-\rho_{11}(t)\end{pmatrix}.$$

The fidelity between two states ρ_s^{α} and ρ_s^{β} is normally defined by $\mathcal{F}(\rho^{\alpha},\rho^{\beta})=(\mathrm{tr}\sqrt{\sqrt{\rho^{\alpha}}\rho^{\beta}\sqrt{\rho^{\alpha}}})^2$. If ρ^{β} is denoted as our prepared state, and $\rho^{\alpha}=|1\rangle\langle 1|$ as our target excited state, then the fidelity can be written as the diagonal component of ρ_s^{β} as $\mathcal{F}(\rho^{\alpha},\rho^{\beta})=\langle 1|\rho^{\beta}|1\rangle=\rho_{11}^{\beta}$. The error may be defined to be $1-\mathcal{F}(\rho^{\alpha},\rho^{\beta})=1-\rho_{11}^{\beta}$; but this definition discards the difference in off-diagonal terms between the prepared state and the target state. If one instead uses the trace distance as the definition for error between the two states $\rho_s^{\alpha}=|1\rangle\langle 1|$ and ρ_s^{β} (degrees of deviation of the prepared state from the target excited state), then one obtains from Eq. (26)

$$D(\rho^{\alpha},\rho^{\beta})=\sqrt{\big(1-\rho_{11}^{\beta}\big)^2+\big|\rho_{12}^{\beta}\big|^2}. \tag{27}$$

One can see that the error definition by the trace distance, Eq. (27), takes the differences in both the diagonal and off-diagonal components into account. If the off-diagonal term ρ_{12}^{β} is ignored, then the trace distance reduces to the error definition of $1-\mathcal{F}(\rho^{\alpha},\rho^{\beta})$. Thus, in the following, we use Eq. (27) as the definition of error for the state preparation.

In principle, we could deal with any given form of the spectral density. But as a particular example, we consider an Ohmic spectral density

$$J(\omega)=\frac{\xi}{2}\omega e^{-\omega/\omega_c}, \tag{28}$$

where ξ is a dimensionless system-bath coupling constant and ω_c is the bath cutoff frequency. The bath correlation function, Eq. (21), is numerically fitted in a multiexponential form as Eq. (22). The minimal number of fitting exponential terms k is chosen to let the value of the squared 2-norm of the residual between Eq. (21) and Eq. (22) be less than or equal to 10^{-7}. Only three to six terms in the expansion are required to fit with CPU time from seconds to minutes regardless of the bath temperature. This is in contrast to the method of the spectral density parametrization [41,44–46] which requires more than 48 exponential terms to express the same bath correlation function at a low temperature of $k_BT=1/\beta=0.2\Omega$ [41]. Through out this paper, the cutoff frequency of $\omega_c=7.5\Omega$ for the bath spectral density is used, and a lower temperature of $k_BT=1/\beta=0.1\Omega$ is chosen such that a higher state preparation fidelity or smaller error can be achieved.

A. Initial state preparations to system-bath thermal equilibrium state

The correlated thermal equilibrium state ρ_T^{eq} of Eq. (6) that will be used as a correlated initial state for Eqs. (23) and (24) up to second order can be obtained by different methods. One method is to calculate $\rho_s(0)$ by directly performing the second-order expansion of Eq. (6) and to calculate $\mathcal{K}_k(0)$ by evaluating the integral of Eq. (20). An alternative method that is simpler is to numerically propagate Eqs. (23) and (24) without the application of any external field from any (factorized) state, say, the first term of Eq. (18), for sufficiently long time to reach equilibrium. Then the reduced system state of the total equilibrium state is $\mathrm{tr}_b(\rho_T^{\mathrm{eq}})=\rho_s(t\to\infty)$ and the corresponding auxiliary equilibrium density matrices are $\mathcal{K}_k^{\mathrm{eq}}=\mathcal{K}_k(t\to\infty)$. Here $t\to\infty$ just means a sufficiently long time at which the system state no longer changes. Then the obtained $\mathrm{tr}_b(\rho_T^{\mathrm{eq}})$ and $\mathcal{K}_k^{\mathrm{eq}}$ will be taken as the initial conditions for the dynamics of the qubit system under the applications of an external driving field. The difference between the results obtained by these two methods for the correlated total thermal equilibrium state of $\mathrm{tr}_b(\rho_T^{\mathrm{eq}})$ and $\mathcal{K}_k^{\mathrm{eq}}$ comes from the fourth-order system-environment coupling which is negligible here [48]. Thus we will adopt the latter numerical method for the preparation of the correlated total equilibrium state.

To demonstrate that this numerical method indeed leads to an equilibrium state, we take $\rho_s(0)=\rho_s(t\to\infty)$ and the nonfactorized part of $\mathcal{K}_k(0)=\mathcal{K}_k^{\mathrm{eq}}$ as the initial conditions for a field-free evolution to compare with the field-free evolutions of other factorized initial states in which $\mathcal{K}_k(0)=0$. We denote ρ_T^{eq} as Initial-A, which is the nonfactorized total thermal

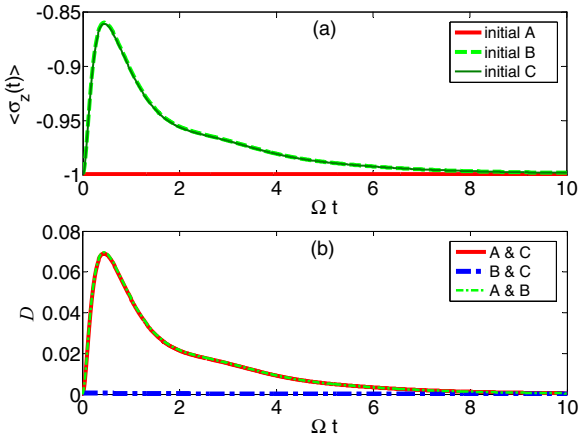

FIG. 1. (a) Field-free time evolutions of $\langle\sigma_z(t)\rangle = \mathrm{tr}_s[\sigma_z\rho_s(t)]$ for different initial states Initial-A: ρ_T^{eq}; Initial-B: $\mathrm{tr}_b(\rho_T^{\mathrm{eq}})\otimes\rho_b$; and Initial-C: $\rho_s^{\mathrm{eq}}\otimes\rho_b$, the first term of Eq. (18). (b) Trace distance between the reduced system states evolving from the different initial states in (a). The line "A & B" denotes the evolution of the trace distance $D(\rho_s^A(t),\rho_s^B(t))$ between the two reduced system states $\rho_s^A(t)$ and $\rho_s^B(t)$ evolving, respectively, from the two initial states Initial-A and Initial-B as shown in (a); similarly for lines "A & C" and "B & C". Other parameters are $\xi = 0.1$, $\omega_c = 7.5\Omega$, and $k_BT = 1/\beta = 0.1\Omega$.

equilibrium state and is obtained by propagating Eqs. (23) and (24) to equilibrium as mentioned above; $\mathrm{tr}_b(\rho_T^{\mathrm{eq}})\otimes\rho_b$ as Initial-B, which is the factorized part of Initial-A in the decomposition of the projection operator P and has the second-order corrections to the reduced system state included; and $\rho_s^{\mathrm{eq}}\otimes\rho_b$ as Initial-C, which is a factorized state with the system and the bath being in their respective individual equilibrium states and is just the first term of Eq. (18). Figure 1(a) shows the time evolution of $\langle\sigma_z(t)\rangle = \mathrm{tr}_s[\sigma_z\rho_s(t)]$ starting from these initial states. One can see that, for the Initial-A state, $\langle\sigma_z(t)\rangle$, as expected, stays the same and does not change at all times, while for the Initial-B and Initial-C states it undergoes an appreciable evolution to different values and eventually reaches the same equilibrium value as that for Initial-A state. The trace distances between the time-dependent states of the reduced system with these initial states are presented in Fig. 1(b). Note that the Initial-A and Initial-B states have the same reduced system density matrix, thus the same initial value of $\langle\sigma_z(0)\rangle = \mathrm{tr}_s[\sigma_z\rho_s(0)]$, and a zero initial trace distance. The corresponding time evolution of the trace distance between the reduced system states in the decomposition of the same initial bath reference state does increase from its initial value, revealing the evidence of the initial correlation [31,34]. The time-dependent trace distance for the two different initial states then diminishes and finally returns, in the long-time limit, to zero, indicating that the reduced system states are the same due to the fact that the corresponding total system-environment states reach equilibrium and become the same. The nearly zero trace distance at all times for the case of "B & C" in Fig. 1(b), in addition to the almost identical time evolution $\langle\sigma_z(t)\rangle$ for the Initial-B and Initial-C states in Fig. 1(a), shows that $\mathrm{tr}_b(\rho_T^{\mathrm{eq}}) = \rho_s(t\to\infty)$ is almost equal to ρ_s^{eq}. This is because the first-order contribution to the system reduced density matrix is zero as $\mathrm{tr}_b[\tilde{H}_{sb}\rho_b] = 0$ and the second-order corrections to the system reduced density matrix vanish in the symmetrical spin-boson model [48] which is just the field-free model we consider. Thus, in the following discussion, Initial-B and Initial-C are regarded as the same and only one of them, the Initial-C state, is employed.

B. State preparations to the excited state

In this section, we will investigate the preparation of the system state to its excited state with an external field using Initial-A and Initial-C states as initial states. This allows us to see the effects of initial correlations on the open-quantum-system dynamics during the state preparation process. Let us first look at the case of the excited state preparation in the closed quantum system (isolated from the environment). The driving Hamiltonian for the state preparation pulse is given in Eq. (5), and a commonly used form with the RWA is

$$H_d^{\mathrm{RWA}}(t) = \frac{\Omega_R}{2}(\sigma_+ e^{-i\omega_L t} + \sigma_- e^{+i\omega_L t}), \tag{29}$$

where $\sigma_\pm = (\sigma_x \pm i\sigma_y)/2$. The RWA works well when the system is driven at resonance or near resonance and the driving strength is weak, that is, when $\omega_L \cong 2\Omega$ and $\Omega_R \ll \Omega$. We will determine the condition for the onset of the non-RWA correction for the excited state preparation later.

For the purpose of the excited state preparation by a single sinusoidal field with frequency ω_L and amplitude Ω_R as in Eq. (5), not all strengths of the field amplitude Ω_R can prepare the qubit system from the ground state to the excited state efficiently and effectively even in the ideal unitary case. When the relevant energy scales of the seemingly simple driven qubit system are in the same order of magnitude, i.e., $\Omega_R \sim \omega_L \sim 2\Omega$, the dynamics becomes complex. Figures 2(a) and 2(b) show the time evolutions of $\langle\sigma_z(t)\rangle$ of the qubit system driven at the resonance frequency $\omega_L = 2\Omega$ with amplitudes $\Omega_R = 2.4\Omega$ and $\Omega_R = 5.0\Omega$, respectively. The complex dynamics in these cases are in contrast with the simple ideal unitary dynamics in the weak-amplitude rotating-wave cases as shown in the inset of Fig. 3(a) for the Initial-D ground state. The first maximum in Fig. 2(a) is not the global maximum and thus requires more time to complete the excited state preparation. This is not efficient and is also more vulnerable when the

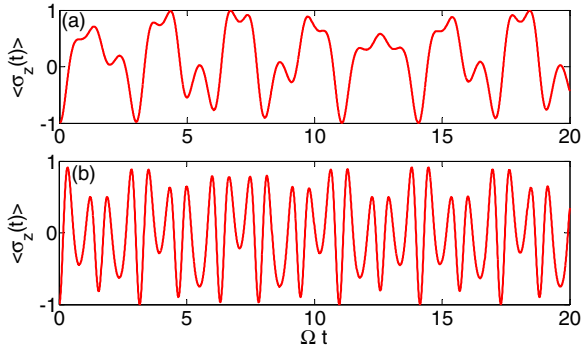

FIG. 2. Unitary time evolutions of $\langle\sigma_z(t)\rangle$ of a two-level system initially in the ground state $|0\rangle\langle 0|$ driven by an external field with the Hamiltonian of Eq. (5) at resonance (i.e., $\omega_L = 2\Omega$) for pulse strengths of (a) $\Omega_R = 2.4\Omega$ and (b) $\Omega_R = 5\Omega$.

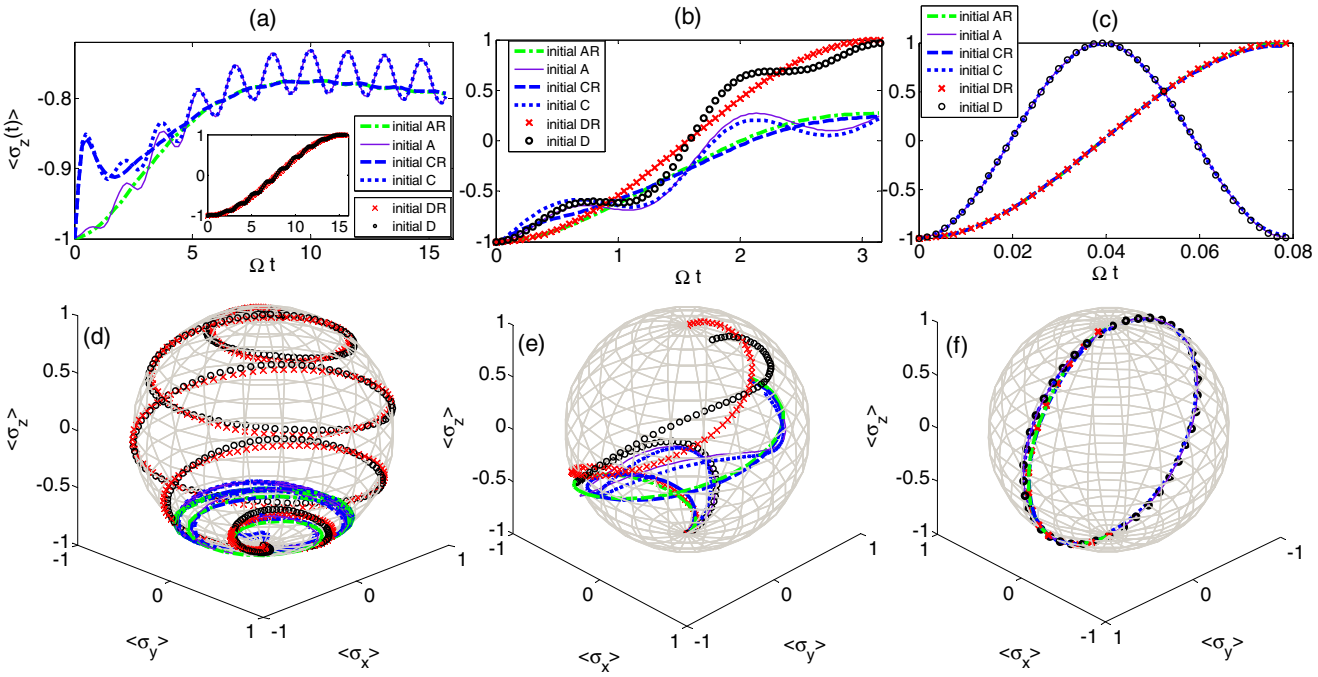

FIG. 3. Time evolutions of $\langle\sigma_z(t)\rangle$ for the excited-state preparations of a two-level system from initial states of Initial-A (thin purple solid line), Initial-C (blue dotted line), and Initial-D (black circle). The Initial-A and Initial-C states are defined in Fig. 1. The time evolution of Initial-D denotes the ideal evolutions from the ground state $|0\rangle\langle 0|$ in the absence of the bath. The evolutions using the pulse of the RWA Hamiltonian Eq. (29) from the same initial states are labeled as Initial-AR (green dot-dashed line), Initial-CR (blue dashed line), and Initial-DR (red cross), respectively. The pulse durations are $t = \pi/\Omega_R$ for different pulse strengths of (a) $\Omega_R = 0.2\Omega$, (b) $\Omega_R = \Omega$, and (c) $\Omega_R = 40\Omega$. The corresponding evolutions of the trajectories in the Bloch sphere representation for (a), (b), and (c) evolving from the south pole to the north pole are shown in (d), (e), and (f), respectively. The evolutions of the states without the RWA in (f) have about a full-round trajectory while the states with the RWA have about a half-round trajectory. Other parameters are $\omega_L = 2\Omega$, $\xi = 0.1$, $\omega_c = 7.5\Omega$, and $k_B T = 1/\beta = 0.1\Omega$.

environment decoherence effect is taken into account. The first maximum in Fig. 2(b) is the global maximum but does not get close to the desired accuracy of the ideal excited state of $\langle\sigma_z\rangle = 1$. Similar complex dynamics are also observed for $\Omega < \Omega_R < 10\Omega$ at resonance, $\omega_L = 2\Omega$. Thus in the following, we confine the amplitude Ω_R of the field for the excited state preparation to be in $0 < \Omega_R \leqslant \Omega$ or $\Omega_R > 10\Omega$.

To demonstrate the conditions for the breakdown of the RWA, we again consider the unitary case first. The RWA predicts that a resonant and weak driving field can transfer the system from the ground state to the excited state in the unitary case with time duration $\Omega_R t = \pi$, the so-called π pulse. In the Bloch sphere representation the system state travels from the south pole $|0\rangle\langle 0|$ ground state to the north pole $|1\rangle\langle 1|$ excited state with a time $t = \pi/\Omega_R$ [1]. In Fig. 3 we show the unitary time evolutions of $\langle\sigma_z(t)\rangle$ and the corresponding Bloch sphere representation of the qubit system for the state preparation from the ground state to the excited state of the system driven at resonance frequency $\omega_L = 2\Omega$ with and without the RWA, denoted as Initial-DR (red cross) and Initial-D (black circle), respectively, for different driving amplitudes. The deviation in the operation time between the cases with and without the RWA increases as Ω_R increases. As shown in Figs. 3(a) and 3(b), the RWA operation time $t = \pi/\Omega_R$ to transfer the two-level system from the ground state to the excited state is good for $\Omega_R \leqslant \Omega$, but the state evolutions with and without the RWA for $\Omega_R = \Omega$ already show considerable difference. For larger value of Ω_R, the precise operation time, that may be hard to calculate analytically, can be deduced numerically when the system state arrives at a place nearest to the north pole. We note that a significant deviation of the operation time from the RWA operation time of $t = \pi/\Omega_R$ can be observed for $\Omega_R \geqslant 10\Omega$. One can see from Fig. 3(c) that the actual operation time is about half of π/Ω_R for $\Omega_R = 40\Omega$. This deviation clearly reflects the failure of the RWA. Of course, this unitary evolution is an ideal case. In reality, it is impossible to completely isolate the system from the environment, so the travel time of the π pulse should be short enough to reduce the effect from the environment such that the arrival position is close to the north pole [49]. Increasing the driving field amplitude Ω_R to shorten the flight time is easier for experiments to perform than changing the system-environment coupling to reduce the environment-induced decoherence and/or decay. But the larger Ω_R is, the less accurate the RWA is.

To see the effect and the overall trend of the RWA and the initial system-environment correlation on the general problem of state preparation, we give in Fig. 4 the errors of the prepared excited states as functions of driving strength Ω_R and the system-bath coupling constant ξ for pulses without and with the RWA and for correlated and factorized initial states. The error of the prepared excited state is defined in Eq. (27). Figure 4(a) shows the error of the prepared states through the non-RWA pulse of the Hamiltonian of Eq. (5) with an initial state Initial-A. The pulse duration is determined for the system state to reach the minimal error at a time around the RWA π-pulse time of $t = \pi/\Omega_R$ in the unitary evolution case.

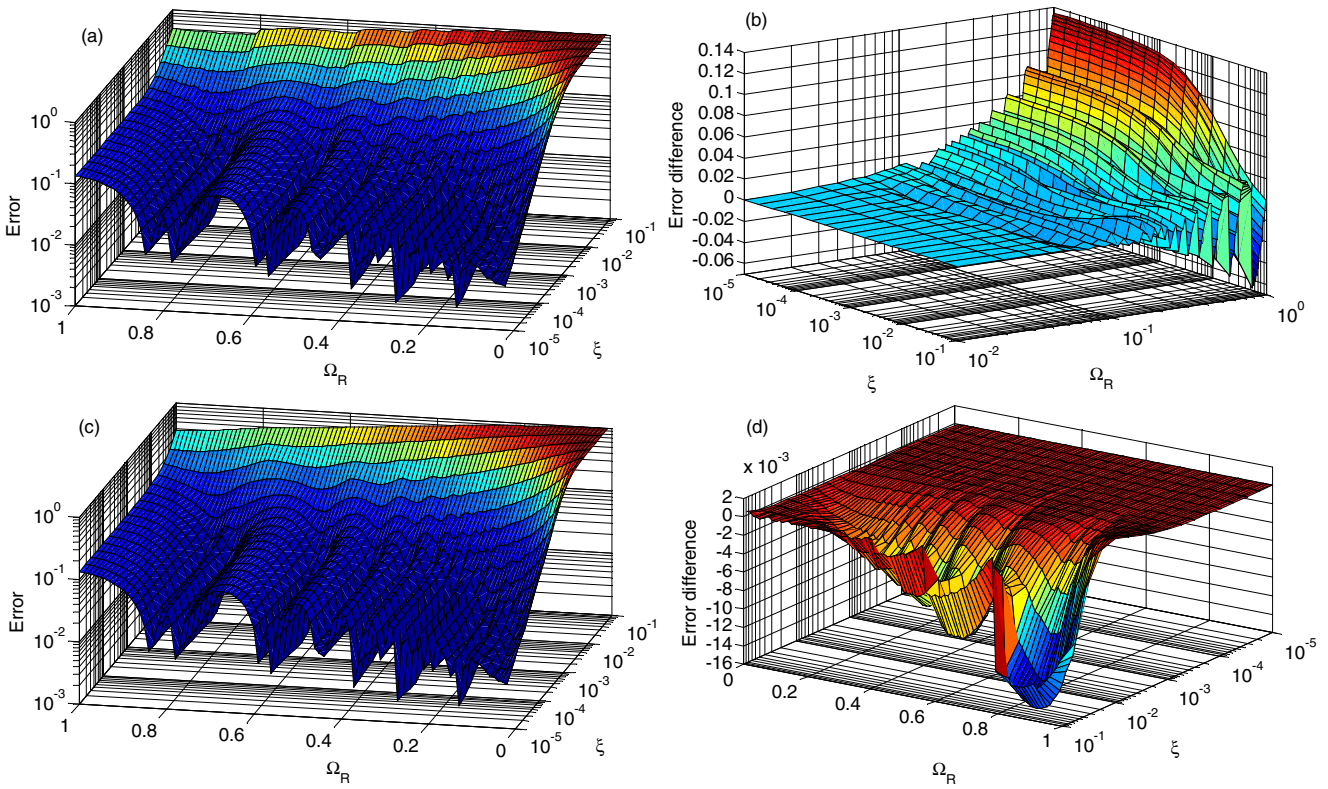

FIG. 4. Error of the excited state preparation as functions of driving strength Ω_R (in unit of Ω) and coupling constant ξ. (a) Error of the prepared excited states by the non-RWA pulse using the Hamiltonian of Eq. (5) from the Initial-A state. Pulse duration is determined by minimizing the error around the time $t = \pi/\Omega_R$ in the ideal unitary evolution. (b) Error difference between the error in (a) and the one by the π pulse of the RWA Hamiltonian of Eq. (29), both starting from the Initial-A state. (c) Error of the prepared excited states by the non-RWA pulse with the same setup as in (a) but with the pulse duration determined by minimizing the error in the open-system case. (d) Error difference between the error in (c) and the error with the same setup and pulse duration as in (c) but with different initial state, Initial-C. Other parameters are $\omega_L = 2\Omega$, $\omega_c = 7.5\Omega$, and $k_B T = 1/\beta = 0.1\Omega$.

One can see from Fig. 4(a) that a higher prepared state fidelity or equivalently a smaller error is achieved as ξ becomes smaller and/or Ω_R becomes larger. However, for $\xi \leqslant 10^{-3}$, the trend of the error increases as Ω_R approaches Ω. This shows that as $\Omega_R \to \Omega$ the somehow complicated non-RWA dynamics raises the error. To compare with the state preparation by the RWA pulse, we give in Fig. 4(b) the error difference between the error in Fig. 4(a) and the one by the RWA π pulse of Eq. (29), both starting from the Initial-A state. If we require the error difference to be smaller than 10^{-2} as a criterion for good agreement between the RWA and non-RWA, then the onset of the non-RWA corrections as seen from Fig. 4(b) takes place at about $\Omega_R \sim 0.1\Omega$.

We can calculate the pulse duration that gives the minimum error between the prepared and target excited states in the open-system case. This fine-tuned pulse duration mimics the pulse length an experimentalist wishes to achieve in a realistic situation. The resultant errors plotted in Fig. 4(c) with slightly smaller error values are quite similar to those of Fig. 4(a), whose pulse durations are calculated in the unitary closed-system case. Figure 4(d) gives the error difference between the errors in Fig. 4(c) and the corresponding errors with the same setup and pulse duration as in Fig. 4(c) but with a different initial state, the factorized Initial-C state. Since the pulse duration is adopted for Initial-A to reach the minimum error, the error difference in Fig. 4(d) is mostly negative. One can also observe that the error difference between the cases of Initial-A and Initial-C start to emerge at about $\xi \geqslant 10^{-2}$. This is due to the fact that the initial system-bath correlation is proportional to ξ, so when ξ reaches a value of about 10^{-2}, the error difference between correlated and factorized initial states becomes visible. Furthermore, the error difference increases as Ω_R increases. This is because small Ω_R requires longer preparation time so that the Initial-C state has enough time to establish system-bath correlations, and then both of the initial states approach the same prepared states. However, as Ω_R increases, the shorter preparation time with smaller pulse duration makes the difference between the corresponding prepared states of the two initial states more appreciable.

We choose a larger coupling constant of $\xi = 0.1$ for the time evolution and the corresponding Bloch sphere plots in Fig. 3 in order to show the breakdowns of the factorization approximation for the initial system-environment state in the open quantum system. The operation times to prepare the excited state are chosen to be the same as the ideal unitary cases to facilitate comparison. One can see from Fig. 3(b) that, after applying the state preparation pulses, the system states, except those in the unitary case, are all far off the target excited state $|1\rangle\langle 1|$, not to mention those of a smaller pulse amplitude in Fig. 3(a). Furthermore, the difference in $\langle \sigma_z(t) \rangle$ between

evolutions with and without the RWA for every initial state in Fig. 3(c) is clearly visible. Observing from Figs. 3(a) and 3(d) as well as from Figs. 3(b) and 3(e), one can conclude that the pulse amplitudes of $\Omega_R = 0.2\Omega$ and $\Omega_R = \Omega$ are too small to transfer those initial states to the excited state for the open quantum system with coupling constant $\xi = 0.1$. Thus larger pulse amplitudes are required as in Fig. 3(c) with a large value of $\Omega_R = 40\Omega$. Figure 3(f) is the evolution trajectory in the Bloch sphere representation for the state preparation process at $\Omega_R = 40\Omega$ of Fig. 3(c). The resultant prepared states with the operation time about $0.5\pi/\Omega_R$ are much closer to the excited state at the north pole of the Bloch sphere than those of the open system cases in Figs. 3(d) and 3(e).

Recognizing already the failure of the RWA Hamiltonian at large pulse amplitudes, we consider only the driving field Hamiltonian without the RWA and plot in Fig. 5 the dynamics of the trace distance between the states evolving from the Initial-A and Initial-C states (abbreviated as "A & C") for the state preparation process with the pulse duration time determined by minimizing the error between the target excited state and the prepared excited state evolving from the Initial-A state, for each value of Ω_R. It is clear that, as the pulse amplitudes Ω_R increases, the operation times for the excited state preparation in the open system become shorter and the resultant prepared states are closer to the excited state $\langle\sigma_z\rangle = 1$. The differences between $\langle\sigma_z(t)\rangle$ evolving from the correlated Initial-A state and from the factorized Initial-C state in Figs. 3(a), 3(b), and 3(c) are hard to recognize, but the corresponding difference in terms of the trace distance can be easily observed in Figs. 5(a), 5(b) and 5(c), respectively, indicating that the trace distance is indeed a sensitive and appropriate measure. We note here that the trace distances under a driving field in Figs. 5(a) and 5(b) increase above their initial values, but the trace distance for "A & C" in Fig. 5(c) (red solid line) decreases initially below its initial value.

The trace distances shown in Fig. 5 also illustrate the difference between the system states evolving from either the Initial-A state (black dashed line) or the Initial-C state (blue dotted line) and from the ideal unitary evolution of the Initial-D state. One can clearly see that, for $\Omega_R = 40\Omega$, the values of the trace distance between states evolving from the Initial-A state and from the Initial-D state (black dashed line) in the whole operation time in Fig. 5(c) are around a small value of order of 10^{-3}, and they are slightly higher for the cases with the Initial-C state at the final time (green dotted line). These small values of the trace distances in Fig. 5(c) as compared to those in the inset of Fig. 5(a) and in Fig. 5(b) demonstrate that large pulse amplitudes are necessary to perform the excited state preparation with the correlated initial state for the system-environment coupling parameter $\xi = 0.1$.

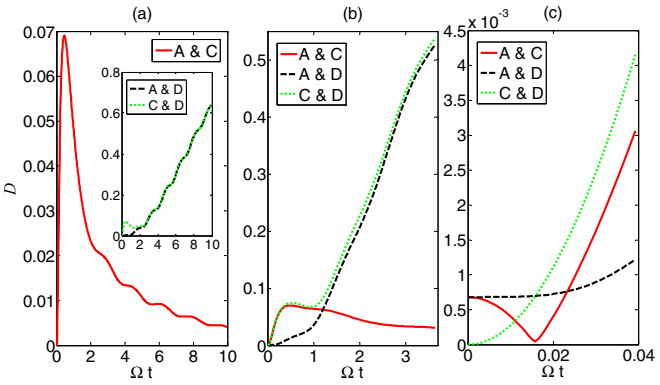

FIG. 5. Time evolutions of the trace distances between the reduced system states evolving from the Initial-A, Initial-C, and Initial-D states, abbreviated as "A & C" (red solid line), "A & D" (black dashed line), and "C & D" (green dotted line), respectively, for different pulse strengths of (a) $\Omega_R = 0.2\Omega$, (b) $\Omega_R = \Omega$, and (c) $\Omega_R = 40\Omega$. The duration of the preparation pulses is obtained by minimizing the error for the open system starting from the Initial-A state for each pulse strength. Other parameters are $\omega_L = 2\Omega, \xi = 0.1$, $\omega_c = 7.5\Omega$, and $k_B T = 1/\beta = 0.1\Omega$.

C. Nonfactorized prepared states after the system state preparation

We next consider the dynamics of the trace distance between these correlated states and their corresponding factorized states in a subsequent field-free evolution. In other words, we take the resultant correlated system-environment states after the state preparation as the initial states for the subsequent field-free evolution. To this end, the values $\rho_s(t)$ and $\mathcal{K}_k(t)$ evolving from the Initial-A and Initial-C states through Eqs. (23) and (24) at the final time of Figs. 5(a), 5(b), and 5(c) (i.e., at the times when the external pulses are turned off) are obtained and denoted as corresponding Prepared-A and Prepared-C states, respectively. Unless there exists possible confusion, we will, for convenience, simply use letters A and C in the following state superscripts and figure legends to represent the Prepared-A and Prepared-C states, respectively. For example, the Prepared-A state is represented by $\rho_s^A = \mathrm{tr}_b(\rho_T^A)$ and $\mathcal{K}_k^A$, and similar notations are applied to the Prepared-C state and other states introduced later. Specifically, the initial input states we will consider in the decomposition by P and Q projection operators for the subsequent field-free evolution are as follows. (i) Prepared-A state: ρ_T^A, correlated state with the reduced system state in the factorized part of the state decomposition being $\rho_s^A = \mathrm{tr}_b(\rho_T^A)$ and the nonfactorized part being $\mathcal{K}_k^A$. (ii) Prepared-A1 state: the factorized part of the Prepared-A state, $\rho_T^{A1} = \rho_s^A \otimes \rho_b$, implying $\mathcal{K}_k^{A1} = 0$. (iii) Prepared-C state: ρ_T^C, a correlated state with the reduced system state in the factorized part being $\rho_s^C = \mathrm{tr}_b(\rho_T^C)$ and the nonfactorized part being $\mathcal{K}_k^C$. (iv) Prepared-C1 state: the factorized part of the Prepared-C state, $\rho_T^{C1} = \rho_s^C \otimes \rho_b$, implying $\mathcal{K}_k^{C1} = 0$. (v) Prepared-D state, the ideal prepared factorized state $|1\rangle\langle 1| \otimes \rho_b$, implying $\mathcal{K}_k^D = 0$.

The results of the trace distance between the reduced system states evolving from these correlated states and their corresponding factorized states in the field-free evolution are presented in Fig. 6. The Prepared-A, -C, and -D states in Fig. 6 are abbreviated simply as A, C, and D states, respectively. The other factorized states of the prepared states are similarly abbreviated. One can find that the values of the trace distance, e.g., "A & C" at the initial time in Figs. 6(a)–6(c), have the same values as those at the final time in Figs. 5(a)–5(c), respectively. The trace distance for "A & C" (red solid line) shown in the inset of Fig. 6(a) is small, less than 5×10^{-3}, indicating that, under the external field with a small pulse amplitude of $\Omega_R = 0.2\Omega$, the long pulse duration allows the factorized

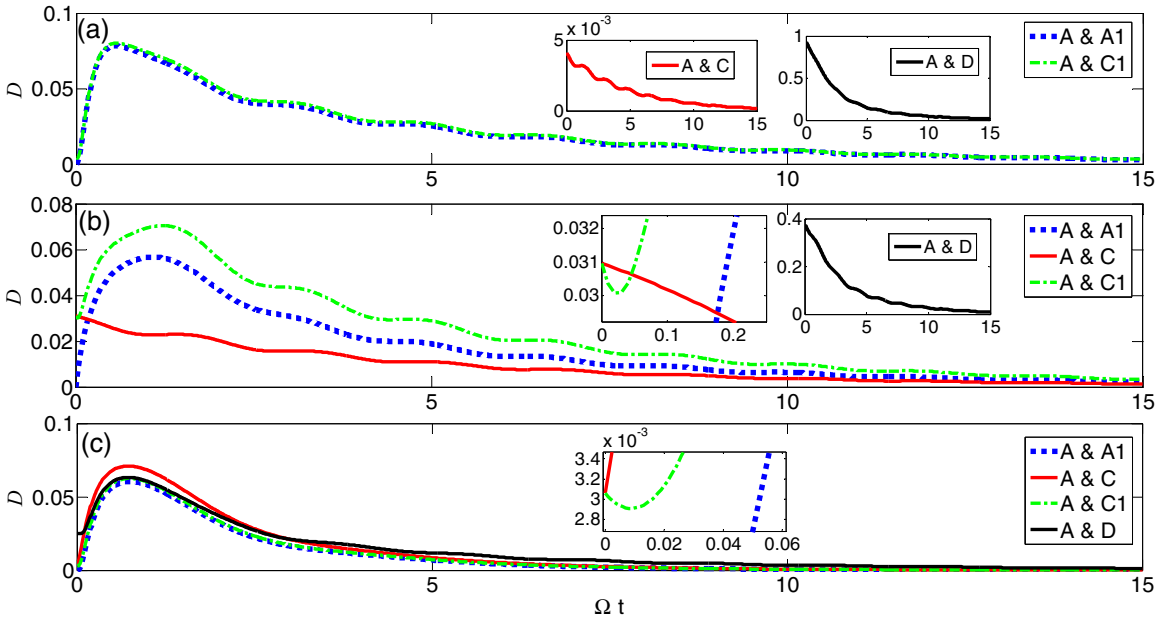

FIG. 6. Field-free evolutions of the trace distances between the reduced system states evolving from several kinds of prepared states for different strengths of (a) $\Omega_R = 0.2\Omega$, (b) $\Omega_R = \Omega$, (c) $\Omega_R = 40\Omega$. The zoom-in plots of the initial evolutions of (b) and (c) are shown in their respective insets. The time evolution of the trace distance between the reduced system states evolving from the Prepared-A and Prepared-A1 states without the external field is abbreviated as "A & A1" (blue dotted line). Similar abbreviations for other time evolutions of the trace distance evolving from their respective prepared states are applied accordingly. Other parameters are $\xi = 0.1$, $\omega_c = 7.5\Omega$, and $k_B T = 1/\beta = 0.1\Omega$.

Initial-C state to establish system-bath correlations such that Prepared-A state and Prepared-C state are almost the same. The decrease of the trace distance from the tiny initial value of the field-free evolution to zero shows that the Prepared-A and Prepared-C states are approaching the same equilibrium state. The trace distance for "A & C" (red solid line) during the course of the excited state preparation with $\Omega_R = 40\Omega$ is also small as shown in Fig. 5(c), but this trace distance grows above its initial value in Fig. 6(c) to larger values in the field-free evolution, in contrast to the decrease in the inset of Fig. 6(a). This is because the short duration of the strong preparation pulse of $\Omega_R = 40\Omega$ makes the factorized Initial-C state evolve only a little bit away from its original state, i.e., just in the beginning stage to establish some system-environment correlation. As a result, one can observe in Fig. 6(c) that the trace distance for "A & C" (red solid line) increases initially and then to a peak value. After that, it decreases and finally approaches zero at long times when the system-bath correlations of "A & C" both reach equilibrium.

The trace distance between the reduced system states evolving from the Prepared-A state and its corresponding factorized part of the Prepared-A1 state (blue dotted line) increases above its initial value for any and all parameter settings in Fig. 6. Because the Prepared-A and Prepared-A1 states are in the decomposition of the same initial bath reference state ρ_b, the increase of the trace distance between them indicates clearly the existence of the initial system-environment correlation. However, the time evolutions of the trace distances other than those of "A & A1" do not always increase above their initial values. See, for example, the zoom-in plots of the initial time evolutions the trace distance "A & C1" as the green dot-dashed line in the insets of Figs. 6(b) and 6(c). We will discuss in some more detail the various dynamical behaviors after we introduce bounds for the trace distance in Sec. V. In Fig. 7 we show the evolution trajectories from the north to the south direction in the Bloch sphere representation with different prepared states as initial states for pulse strengths of $\Omega_R = \Omega$ and $\Omega_R = 40\Omega$, corresponding to those in Figs. 6(b) and 6(c), respectively.

V. BOUNDS FOR THE TRACE DISTANCE: ROLE OF THE SYSTEM-ENVIRONMENT CORRELATIONS

To gain a quantitative understanding of the diverse behavior of the trace distance in general, we present an analysis that bounds the finite-time difference in trace distance by sharply defined quantities that link to the existence of the system-environment correlation in Sec. V A. We will then take the field-free case in Fig. 6 as an example to find and analyze the upper and lower bounds in Sec. V B. Similar bounds using another form of the initial bath reference state are discussed in Ref. [34].

A. Upper and lower bounds

The trace distance between two different reduced system states $\rho_s^\alpha(t',t)$ and $\rho_s^\beta(t',t)$ of a given open quantum system evolving from time t' to t can be written as

$$D(t',t,\rho^{\alpha,\beta}) = D\big(\rho_s^\alpha(t',t),\rho_s^\beta(t',t)\big) = \frac{1}{2}\big\|\mathrm{tr}_b\big\{\mathcal{G}_T(t,t')\Delta\rho_T^{\alpha,\beta}(t')\big\}\big\|, \quad (30)$$

where $\Delta\rho_T^{\alpha,\beta}(t') = \rho_T^\alpha(t') - \rho_T^\beta(t')$. Any joint system-environment state $\rho_T(t)$ can be decomposed by the P and Q projection operators as the expression of Eq. (7). Thus one has $\Delta\rho_T^{\alpha,\beta}(t') = \Delta\rho_s^{\alpha,\beta}(t') \otimes \rho_b + Q\Delta\rho_T^{\alpha,\beta}(t')$, where

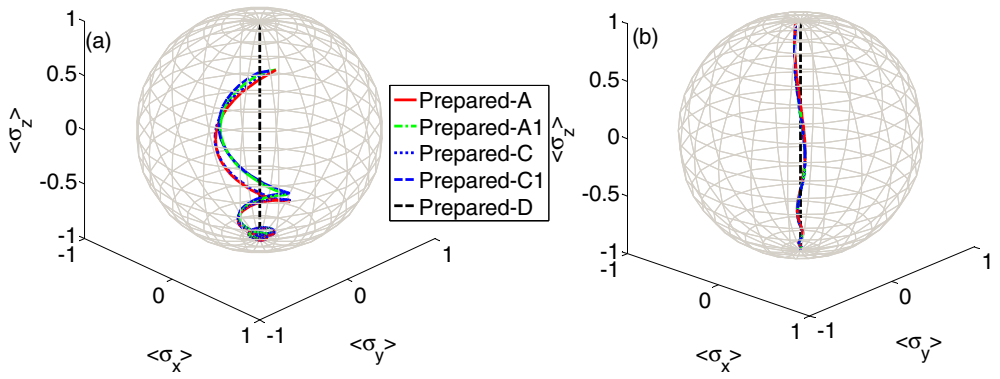

FIG. 7. Field-free evolutions of the trajectories evolving from the north to the south direction in the Bloch sphere representation with different prepared states as initial states for different pulse strengths of (a) $\Omega_R = \Omega$ and (b) $\Omega_R = 40\Omega$, corresponding to the time evolutions of the system in Figs. 6(b) and 6(c), respectively.

$\Delta\rho_s^{\alpha,\beta}(t') = \rho_s^{\alpha}(t') - \rho_s^{\beta}(t') = \mathrm{tr}_b[\rho_T^{\alpha}(t') - \rho_T^{\beta}(t')]$. Substituting the above expression into Eq. (30) and using the triangular inequality for the trace norm,

$$\|\Gamma\| + \|\Gamma'\| \geqslant \|\Gamma + \Gamma'\| \geqslant |\|\Gamma\| - \|\Gamma'\||, \tag{31}$$

where Γ and Γ' are linear trace class operators, we obtain bounds to the trace distance $D(t',t,\rho^{\alpha,\beta})$:

$$\begin{aligned} &I(t',t,\rho^{\alpha,\beta}) + F(t',t,\rho^{\alpha,\beta}) \\ &\quad\geqslant D(t',t,\rho^{\alpha,\beta}) \geqslant |I(t',t,\rho^{\alpha,\beta}) - F(t',t,\rho^{\alpha,\beta})|, \end{aligned} \tag{32}$$

where

$$F(t',t,\rho^{\alpha,\beta}) = \tfrac{1}{2}\left\|\mathrm{tr}_b\left\{\mathcal{G}_T(t,t')\left[\Delta\rho_s^{\alpha,\beta}(t')\otimes\rho_b\right]\right\}\right\|, \tag{33}$$

$$I(t',t,\rho^{\alpha,\beta}) = \tfrac{1}{2}\left\|\mathrm{tr}_b\left\{\mathcal{G}_T(t,t')\left[Q\Delta\rho_T^{\alpha,\beta}(t')\right]\right\}\right\|. \tag{34}$$

The quantity $F(t',t,\rho^{\alpha,\beta})$ in Eq. (33) is the trace distance between two reduced system states at time t, which evolved from their respective total system-bath product states at an earlier time t'. One can describe the time evolution of the reduced system in $F(t',t,\rho^{\alpha,\beta})$ through a family of completely positive dynamical maps. Completely positive maps with the same initial environment state are contractive and they form a time-dependent semigroup, and so they are Markovian quantum stochastic processes [36,37]. This is why the concepts of no initial correlation, complete positive maps, contractivity, and Markovianity are often linked or discussed all together in the literature. Contractivity means that the distinguishability of two input states cannot increase in time, i.e., the trace distance of the system density matrices of the quantum process decreases with time. Thus one has $F(t',t,\rho^{\alpha,\beta}) \leqslant F(t',t',\rho^{\alpha,\beta})$ due to the contractive property of the completely positive maps with the same initial environment states. The quantity $I(t',t,\rho^{\alpha,\beta})$ in Eq. (34) keeps track of the effect of the system-bath correlation at a time t' on the subsequent dynamics of the reduced system at time t. Since the propagator superoperator $\mathcal{G}_T(t',t') = 1$ and the property $\mathrm{tr}_b[Q\rho_T(t')] = 0$ (due to $PQ = 0$), one has at the initial propagating time t' the quantity $I(t',t',\rho^{\alpha,\beta}) = 0$. In general, $I(t',t,\rho^{\alpha,\beta})$ depends on the system-bath correlations established at time t' for each of $Q\rho_T^{\alpha}(t')$ and $Q\rho_T^{\beta}(t')$. If there are no system-bath correlations at time t', i.e., $Q\rho_T^{\alpha}(t') = 0 = Q\rho_T^{\beta}(t')$, or if there are system-bath correlations but their difference vanishes at time t', i.e., $Q\Delta\rho_T^{\alpha,\beta}(t') = 0$, then $I(t',t,\rho^{\alpha,\beta}) = I(t',t',\rho^{\alpha,\beta}) = 0$. Thus $I(t',t,\rho^{\alpha,\beta}) > I(t',t',\rho^{\alpha,\beta}) = 0$ can serve as an indicator of whether there is difference of the initial correlations at time t' between the two total states, i.e., whether $Q\Delta\rho_T^{\alpha,\beta}(t') \neq 0$.

Witnesses of non-Markovianity through detecting deviations from contractive dynamics have been proposed and investigated [15,26,32,42,43]. Based on these investigations, if a process is not contractive (or the trace distance of a process increases) at some instant time or in some time intervals for some states, then the process is non-Markovian. Thus it is instructive to find the necessary condition and the sufficient condition for the increase of the trace distance in the time interval $[t',t]$. Again, since $I(t',t',\rho^{\alpha,\beta}) = 0$, one has $D(t',t',\rho^{\alpha,\beta}) = F(t',t',\rho^{\alpha,\beta})$. Thus by using these relations, the necessary condition for the increase of the trace distance $D(t',t,\rho^{\alpha,\beta}) > D(t',t',\rho^{\alpha,\beta})$ is then the increase of the upper bound in Eq. (32),

$$I(t',t,\rho^{\alpha,\beta}) + F(t',t,\rho^{\alpha,\beta}) > I(t',t',\rho^{\alpha,\beta}) + F(t',t',\rho^{\alpha,\beta}), \tag{35}$$

and the sufficient condition is the increase of the lower bound in Eq. (32),

$$\begin{aligned} &|I(t',t,\rho^{\alpha,\beta}) - F(t',t,\rho^{\alpha,\beta})| \\ &\quad> |I(t',t',\rho^{\alpha,\beta}) - F(t',t',\rho^{\alpha,\beta})|. \end{aligned} \tag{36}$$

If the value of $I(t',t,\rho^{\alpha,\beta})$ makes the sufficient condition, Eq. (36), satisfied for *some* choice of t',t and $\rho^{\alpha}(t'),\rho^{\beta}(t')$, then the dynamics is non-Markovian. If, however, the value of $I(t',t,\rho^{\alpha,\beta})$ satisfies the condition [opposite to the necessary condition of Eq. (35)]

$$I(t',t,\rho^{\alpha,\beta}) + F(t',t,\rho^{\alpha,\beta}) < I(t',t',\rho^{\alpha,\beta}) + F(t',t',\rho^{\alpha,\beta}) \tag{37}$$

for *all* choices of t',t and $\rho^{\alpha}(t'),\rho^{\beta}(t')$, the dynamics is Markovian.

Similar bounds of the finite-time difference in trace distance and forms of the necessary condition and sufficient condition for the increase of the trace distance can be found in Ref. [34]. However, the decomposition of a general joint system-environment state in Ref. [34] is through the reduced states of the system and the reduced state of the environment

[28,33,34]:

$$\rho_T(t) = \rho_s(t) \otimes \rho_e(t) + \chi_{se}(t), \tag{38}$$

where $\rho_e(t) = \mathrm{tr}_s[\rho_T(t)]$ is the reduced state of the environment at time t and $\chi_{se}(t)$ accounts for the remaining correlations between the open system and the environment. This decomposition is different from the decomposition of Eq. (7) using the projection operators P and Q. The reference bath state is the fixed bath thermal equilibrium state ρ_b for all total system-environment states in our formulation, while the reduced environment states $\rho_e(t)$ in Ref. [34] are time-dependent and are different for different total system-environment states. As a consequence, the remaining system-bath correlations in these two decompositions are also different. The disadvantage of the decomposition of Eq. (38) is that it is hard to calculate the corresponding bounds presented in Ref. [34] unless an exact dynamical solution of the total system-bath state is available to evaluate the time-dependent reduced state of the environment. In contrast, our decomposition of Eq. (7) can be directly combined with the perturbative master equation approach by the projection operator technique even with strong external driving fields for the calculation of the dynamics of the derived corresponding bounds of the trace distance.

B. Examples of the field-free evolutions for the upper and lower bounds

Next we present the time evolutions of the $I(t',t,\rho^{\alpha,\beta})$ and $F(t',t,\rho^{\alpha,\beta})$ of Eqs. (33) and (34) for the upper and lower bounds in Eq. (32). We will take the diverse behaviors of the dynamics of the trace distances presented in Fig. 6 as examples to illustrate that they are indeed within the bounds. Compared to Eqs. (10) and (30), Eqs. (33) and (34) satisfy the same equation of motion of Eq. (12) as Eq. (30) but with different initial conditions. To second order in the system-environment interaction Hamiltonian, this same equation of motion can be cast into the master equation of Eqs. (23) and (24) in the extended auxiliary Liouville space. The initial condition for $F(t',t,\rho^{\alpha,\beta})$ is $F(t',t',\rho^{\alpha,\beta}) = \frac{1}{2}\|\Delta\rho_s^{\alpha,\beta}(t')\|$, and the initial inputs in terms of the extended Liouville space formulation become $\rho_s^{\alpha,\beta}(t')$ and $\mathcal{K}_k^{\alpha,\beta}(t') = 0$. Similarly, the initial condition for $I(t',t,\rho^{\alpha,\beta})$ is $I(t',t',\rho^{\alpha,\beta}) = 0$, and in the extended Liouville space formulation the initial inputs are $\rho_s^{\alpha,\beta}(t') = 0$ and $\mathcal{K}_k^{\alpha,\beta}(t')$ that correspond to $Q\rho_T^{\alpha,\beta}(t')$.

Figure 8 shows the dynamics of the trace distance $D(t' = 0,t,\rho^{A,C(C1)})$ between the reduced system states evolving from the Prepared-A and Prepared-C (Prepared-C1) states in the field-free case after the application of the preparation pulse with different pulse amplitudes. We have set the time when the external preparation pulse is turned off as t' and relabeled it as $t' = 0$. We also plot in Fig. 8 the quantities $I(0,t,\rho^{A,C(C1)})$ (green solid line), $F(0,t,\rho^{A,C(C1)})$ (black dotted line), and the corresponding upper (blue dashed line) and lower (blue dot-dashed line) bounds of the trace distance. The dynamical behaviors of the trace distances shown in Fig. 6 and Fig. 8 are quite diverse. The time evolution of the trace distance of "A & C", the red solid line in Fig. 8(a), shows nonmonotonic decrease from its initial value (indicating a witness of non-Markovianity), while that in Fig. 6(c) increases above its initial value (indicating a witness of an initial correlation), reaches a peak and then decreases. The trace distances of "A & C1" in red solid lines in Figs. 8(b) and 8(c) decrease at first below their initial values (see the zoom-in plots of the initial time

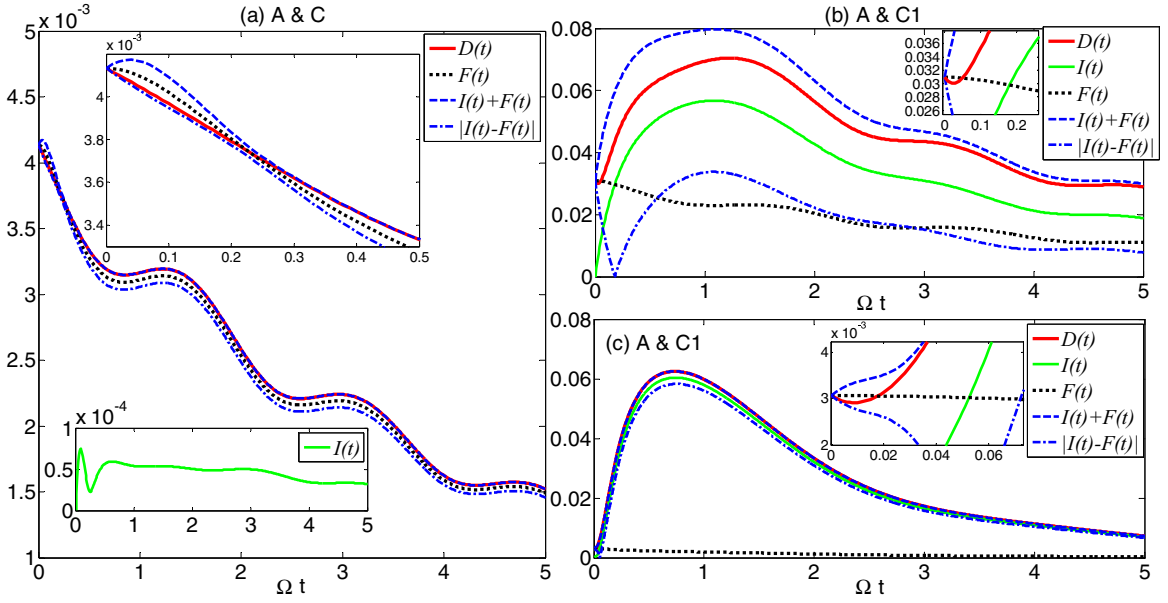

FIG. 8. Field-free evolutions of the trace distance (red solid line) and corresponding upper (blue dashed line) and lower (blue dot-dashed line) bounds in Eq. (32). The trace distances $D(t' = 0,t,\rho^{A,C(C1)})$ between the reduced system states evolving from the Prepared-A and Prepared-C (Prepared-C1) states after the application of the preparation pulse are abbreviated as $D(t)$ for "A & C (C1)", shown as red solid lines. The different pulse amplitudes and trace distances shown are (a) "A & C" with $\Omega_R = 0.2\Omega$, (b) "A & C1" with $\Omega_R = \Omega$, and (c) "A & C1" with $\Omega_R = 40\Omega$. The zoom-in plots of the initial evolutions of (a), (b), and (c) are shown in their respective insets. Here the time t' when the external preparation pulse is turned off is relabeled as $t' = 0$. The time evolutions of the quantities $I(0,t,\rho^{A,C(C1)})$ and $F(0,t,\rho^{A,C(C1)})$ for "A & C (C1)" abbreviated as $I(t)$ (green solid line) and $F(t)$ (black dotted line), respectively, are also presented.

evolutions in the insets), but then increase above their initial values and later decrease again. One can observe that the time evolutions of the trace distance, no matter how diverse their behaviors, are all between the bounds satisfying Eq. (32). For example, the trace distance $D(0,t,\rho^{A,C1})$ in Fig. 8(c) is close to the upper bound for almost all the period of time shown but is still within the bounds. The question about whether or how the trace distances are close to the upper or lower bounds depends on what the two reduced system states and the nonfactorized parts are in Eq. (32). We find that the trace distance $D(0,t,\rho^{A,C1})$ in Fig. 8(b) will change its behavior from being around the middle of the bounds to oscillating closely to the upper or the lower bound if one changes the duration time of the preparation pulse prior to the field-free evolution, with other conditions and parameters unchanged.

Even though the effect of the system-environment correlation increases $I(0,t,\rho^{\alpha,\beta}) > I(0,0,\rho^{\alpha,\beta}) = 0$, the trace distance between the reduced system states does not always increase above its initial value. An increase of the trace distance (distinguishability) between the reduced states, however, requires $I(0,t,\rho^{\alpha,\beta})$ to prevail over the difference of $[F(0,0,\rho^{\alpha,\beta}) - F(0,t,\rho^{\alpha,\beta})]$, the amount of contraction due to the completely positive maps. Indeed, whenever $D(0,t,\rho^{\alpha,\beta})$ increases above its initial values in Figs. 8(b) and 8(c), the necessary condition, Eq. (35), is always satisfied. It is only when the initial $F(0,0,\rho^{\alpha,\beta}) = 0$ [implying $F(0,t,\rho^{\alpha,\beta}) = 0$] that the trace distance increases above its initial value once $I(0,t,\rho^{\alpha,\beta}) > 0$. This follows from the sufficient condition, Eq. (36). If the two initial states ρ^{α} and ρ^{β} are chosen to be, respectively, a correlated state and its corresponding factorized state with the same reduced system state, such as the Prepared-A and Prepared-A1 states, then $F(0,0,\rho^{\alpha,\beta}) = 0 = F(0,t,\rho^{\alpha,\beta})$ and $I(0,t,\rho^{\alpha,\beta}) > 0$ [note that $I(0,t \to \infty,\rho^{\alpha,\beta}) \to 0$]. This explains why, in Fig. 6, an increase of the trace distance $D(0,t,\rho^{A,A1})$ over its initial value always takes place. There exist some certain times of about $t > 0.07/\Omega$ in Fig. 8(c) that $I(0,t,\rho^{A,C1})$ is not only greater than zero but also large enough to make the sufficient condition, Eq. (36), satisfied. Thus in this case, $D(0,t,\rho^{A,C1})$ is guaranteed to increase over its initial value for times $t > 0.07/\Omega$ although $D(0,t,\rho^{A,C1})$ actually increases over its initial value at an earlier time about $t = 0.02/\Omega$.

VI. CONCLUSION

We have investigated the problem of system state preparation by an external field in the presence of an environment with initial system-environment correlations. The open-quantum-system model we consider is a spin-boson model and the target system state we wish to prepare is the excited state of the two-level system (or the spin). Starting with an initial joint system-environment state in the correlated total thermal equilibrium state, we use the projection operator technique to obtain a perturbative time-nonlocal master equation for the reduced system density matrix, which takes into account the effect of the initial system-environment correlation. To describe the dynamics of the system under the application of a time-dependent external (strong) field, one would need to solve the master equation that is a time-nonlocal, time-ordered integro-differential equation. Instead of solving the quantum master equation directly, we express the bath correlation function in a multiexponential form and transform the time-nonlocal and time-ordered integro-differential equation into a set of coupled linear time-local differential equations in an extended auxiliary Liouville space. The resultant coupled differential equations, that are time-local and have no time-ordering and memory kernel integration problems, are much easier to solve. Moreover, these coupled equations take into account the initial system-environment correlation and can deal with the case of strong driving fields with which the RWA breaks down.

We have used the time evolutions of $\langle\sigma_z(t)\rangle$, the trace distance, and the trajectory in the Bloch sphere representation to study the effects of the initial system-environment correlations, the amplitudes of the preparation pulses, and the strengths of system-environment couplings on the system state preparation. We have found that, unless the system-bath coupling is very weak as compared to the pulse amplitude Ω_R, it is hard to perform the high-fidelity system state preparation with a single resonant sinusoidal field. For the model and parameters discussed in this paper, when the system-bath coupling constant $10^{-5} \leqslant \xi \leqslant 10^{-3}$ and $0.01 < (\Omega_R/\Omega) < 0.8$, the error of the excited state preparation can be less than 10^{-2}. For a slightly larger value of the system-bath coupling and considering the initial system-environment state to be in the total thermal equilibrium state, a larger value of Ω_R is required. When Ω_R is not very small comparing to the frequency of the two-level system Ω, the commonly adopted RWA fails. We have found that the onset of the non-RWA corrections takes place at about $\Omega_R \sim 0.1\Omega$ where the error difference of the excited state preparation between the RWA and non-RWA cases is about 10^{-2}. We have also investigated the case when Ω_R is much larger than Ω. We have also found that the state preparation error of the initial factorization approximation for the total system-bath states starts to show deviation from that of the correlated case when the system-bath coupling constant $\xi > 10^{-2}$.

We have introduced more computable upper and lower bounds for the trace distance between two reduced system states in a decomposition of the total system-environment states with a fixed reference thermal environment state by the projection operators P and Q. These bounds give a sufficient condition and a necessary condition for the increase of the trace distance and are related to the witnesses of non-Markovianity and of the difference in initial system-environment correlations. We have used these upper and lower bounds to describe the diverse behaviors of the field-free time evolutions of the trace distance between reduced system states evolving from various correlated and uncorrelated states right after the state preparation pulses are turned off. These upper and lower bounds, that can be calculated through the perturbative master equation approach, can be directly applied to a wide range of open system models to study problems such as the state distinguishability, the effects of initial system-bath correlations, and their corresponding dynamics.

ACKNOWLEDGMENTS

We acknowledge support from the Ministry of Science and Technology, Taiwan, under Grant No. 103-2112-M-002-

003-MY3, from the National Taiwan University under Grant No. NTU-ERP-104R891402, and from the thematic group program of the National Center for Theoretical Sciences, Taiwan.

[1] H. J. Carmichael, *Statistical Methods in Quantum Optics 1* (Springer, Berlin, 1999).
[2] H. P. Breuer and F. Petruccione, *The Theory of Open Quantum Systems* (Oxford University Press, Oxford, 2002).
[3] Á. Rivas and S. F. Huelga, *Open Quantum Systems: An Introduction* (Springer, Heidelberg, 2012).
[4] C. F. Li, J. S. Tang, Y. L. Li, and G. C. Guo, Phys. Rev. A **83**, 064102 (2011).
[5] A. Smirne, D. Brivio, S. Cialdi, B. Vacchini, and M. G. A. Paris, Phys. Rev. A **84**, 032112 (2011).
[6] M. Ringbauer, C. J. Wood, K. Modi, A. Gilchrist, A. G. White, and A. Fedrizzi, Phys. Rev. Lett. **114**, 090402 (2015).
[7] A. M. Kuah, K. Modi, C. A. Rodríguez-Rosario, and E. C. G. Sudarshan, Phys. Rev. A **76**, 042113 (2007); K. Modi and E. C. G. Sudarshan, *ibid.* **81**, 052119 (2010).
[8] K. Modi, Open Syst. Inf. Dyn. **18**, 253 (2011).
[9] A. Z. Chaudhry and J. B. Gong, Phys. Rev. A **87**, 012129 (2013).
[10] A. Z. Chaudhry and J. B. Gong, Phys. Rev. A **88**, 052107 (2013).
[11] P. Pechukas, Phys. Rev. Lett. **73**, 1060 (1994).
[12] A. Royer, Phys. Rev. Lett. **77**, 3272 (1996).
[13] M. Campisi, P. Talkner, and P. Hänggi, Phys. Rev. Lett. **102**, 210401 (2009).
[14] A. G. Dijkstra and Y. Tanimura, Phys. Rev. Lett. **104**, 250401 (2010).
[15] A. G. Dijkstra and Y. Tanimura, Philos. Trans. R. Soc. A **370**, 3658 (2012).
[16] C. K. Lee, J. S. Cao, and J. B. Gong, Phys. Rev. E **86**, 021109 (2012).
[17] H. A. Carteret, D. R. Terno, and K. Życzkowski, Phys. Rev. A **77**, 042113 (2008).
[18] K. Modi, C. A. Rodríguez-Rosario, and A. Aspuru-Guzik, Phys. Rev. A **86**, 064102 (2012).
[19] F. Buscemi, Phys. Rev. Lett. **113**, 140502 (2014).
[20] L. Liu and D. M. Tong, Phys. Rev. A **90**, 012305 (2014).
[21] J. M. Dominy, A. Shabani, and D. A. Lidar, Quantum Inf. Process. **15**, 465 (2016).
[22] M. Ban, Phys. Rev. A **80**, 064103 (2009).
[23] C. Uchiyama and M. Aihara, Phys. Rev. A **82**, 044104 (2010).
[24] A. Smirne, H-P. Breuer, J. Piilo, and B. Vacchini, Phys. Rev. A **82**, 062114 (2010).
[25] Y. J. Zhang, X.-B. Zou, Y.-J. Xia, and G.-C. Guo, Phys. Rev. A **82**, 022108 (2010).
[26] J. Dajka and J. Łuczka, Phys. Rev. A **82**, 012341 (2010); J. Dajka, J. Łuczka, and P. Hänggi, *ibid.* **84**, 032120 (2011).
[27] V. G. Morozov, S. Mathey, and G. Röpke, Phys. Rev. A **85**, 022101 (2012).
[28] C. Uchiyama, Phys. Rev. A **85**, 052104 (2012).
[29] Y. Gao, Eur. Phys. J. D **67**, 183 (2013).
[30] V. Semin, I. Sinayskiy, and F. Petruccione, Phys. Rev. A **86**, 062114 (2012).
[31] E. M. Laine, J. Piilo, and H.-P. Breuer, Europhys. Lett. **92**, 60010 (2010).
[32] C. A. Rodríguez-Rosario, K. Modi, L. Mazzola, and A. Aspuru-Guzik, Europhys. Lett. **99**, 20010 (2012).
[33] L. Mazzola, C. A. Rodríguez-Rosario, K. Modi, and M. Paternostro, Phys. Rev. A **86**, 010102(R) (2012).
[34] A. Smirne, L. Mazzola, M. Paternostro, and B. Vacchini, Phys. Rev. A **87**, 052129 (2013).
[35] Á. Rivas, S. F. Huelga, and M. B. Plenio, Rep. Prog. Phys. **77**, 094001 (2014), and references therein.
[36] V. Gorini, A. Kossakowski, and E. C. G. Sudarshan, J. Math. Phys. **17**, 821 (1976).
[37] G. Lindblad, Commun. Math. Phys. **48**, 119 (1976).
[38] N. Erez, G. Gordon, M. Nest, and G. Kurizki, Nature (London) **452**, 724 (2008).
[39] G. Gordon, G. Bensky, D. Gelbwaser-Klimovsky, D. D. Rao, N. Erez, and G. Kurizki, New J. Phys. **11**, 123025 (2009).
[40] G. Gordon, D. D. Rao, and G. Kurizki, New J. Phys. **12**, 053033 (2010).
[41] C. Meier and D. J. Tannor, J. Chem. Phys. **111**, 3365 (1999).
[42] X. Wang and S. G. Schirmer, Phys. Rev. A **79**, 052326 (2009).
[43] H.-P. Breuer, E.-M. Laine, and J. Piilo, Phys. Rev. Lett. **103**, 210401 (2009).
[44] R. X. Xu and Y. J. Yan, J. Chem. Phys. **116**, 9196 (2002).
[45] U. Kleinekathöfer, J. Chem. Phys. **121**, 2505 (2004).
[46] A. Pomyalov, C. Meier, and D. J. Tannor, Chem. Phys. **370**, 98 (2010).
[47] B. Hwang and H. S. Goan, Phys. Rev. A **85**, 032321 (2012); J.-S. Tai, K.-T. Lin, and H.-S. Goan, *ibid.* **89**, 062310 (2014).
[48] E. Geva, E. Rosenman, and D. Tannor, J. Chem. Phys. **113**, 1380 (2000).
[49] C. H. Fleming, A. Roura, and B. L. Hu, Phys. Rev. E **84**, 021106 (2011).